PCCP

Accepted Manuscript

This is an *Accepted Manuscript*, which has been through the Royal Society of Chemistry peer review process and has been accepted for publication.

Accepted Manuscripts are published online shortly after acceptance, before technical editing, formatting and proof reading. Using this free service, authors can make their results available to the community, in citable form, before we publish the edited article. We will replace this *Accepted Manuscript* with the edited and formatted *Advance Article* as soon as it is available.

You can find more information about *Accepted Manuscripts* in the **Information for Authors**.

Please note that technical editing may introduce minor changes to the text and/or graphics, which may alter content. The journal's standard **Terms & Conditions** and the **Ethical guidelines** still apply. In no event shall the Royal Society of Chemistry be held responsible for any errors or omissions in this *Accepted Manuscript* or any consequences arising from the use of any information it contains.

PCCP

ARTICLE

Synthesis, phase composition, Mössbauer and magnetic characterizations of iron oxide nanoparticles

Sarveena,[a] J. M. Vargas,[b] D. K. Shukla,[c] C. T. Meneses,[d] P. Mendoza Zélis,[e] M. Singh,[a] and S. K. Sharma[f, a*]

The present work describes the synthesis of iron oxide nanoparticles by thermal decomposition of Fe-precursors in argon and vacuum environments with control over particle size distribution, phase composition and the resulting magnetic properties. The Rietveld analysis of X-ray diffraction data revealed the crystallinity as well single-phase γ-Fe$_2$O$_3$ nanoparticles prepared under vacuum, whereas argon environment leads to the formation of multi-phase composition of γ-Fe$_2$O$_3$/Fe$_3$O$_4$ (90%) and wustite (10%). Synchrotron x-ray absorption near edge structure (XANES) indicates that the predominant phase in both the samples is γ-Fe$_2$O$_3$, which is subsequently verified from the Mössbauer spectra. DC magnetic measurements indicate behavior typical of superparamagnetic system validated by Mössbauer analysis. However, further investigation of ac susceptibility by typical Néel-Arrhenius and Vogel Fulcher magnetic models suggest an influence from interparticle interactions on the overall magnetic behavior of the system.

Introduction

Magnetic iron oxide based nanoparticles have become the center of huge attraction among the scientific community because of their increasing number of applications in various fields [1]. Recently, much attention has been paid towards the superparamagnetic Fe$_3$O$_4$nanoparticles not because of their complex magnetic behavior, but also their suitability in various biological applications [2-3]. However, one of the most significant tasks in the synthesis of iron oxide nanoparticles is the control over the phase purity, which hinders to distinguish between pure magnetite and maghemite phase, as their crystal structures are very close. Furthermore, Fe$_3$O$_4$ has been predicted to be half metallic at 300 K and hence is expected to produce 100% spin polarization of an electric current passing through [4]. Thin films of Fe$_3$O$_4$ nanoparticles have been shown to display very interesting magneto-resistance values in comparison to thin films prepared by physical methods and are expected to lead to the development of magneto-electronic devices with enhanced magneto-transport properties [5]. Beside these, at nanoscale regime, Fe^{2+}, in Fe$_3$O$_4$ ([Fe^{3+}]$_A$ [Fe^{3+}Fe^{2+}]$_B$O$_4$ with A- and B- so called tetrahedral and octahedral sites, becomes very sensitive

to oxidation state hence may change the nanoparticle composition and properties, particularly at the surface. Therefore, the reproducibility of iron oxide nanoparticle (IONPs) with desired controlled phase compositions and magnetic properties is a challenging task, and equally important from applications point of view. In this regards, researchers are trying to optimize the synthesis conditions leading to reproducible sizes and compositions and hence the desired magnetic properties of nanoparticles. Moreover, a very important issue is to better understand the synthesis recipe in order to have a better control over the size/shape distribution and hence to establish a good relation with size and structure dependent magnetic properties.

Different synthesis strategies have been found in the literature for obtaining the iron oxide nanoparticles with well-defined size/shape and phase composition [6-8].However, among these, the synthesis by thermal decomposition of metal precursor in a high boiling solvent appears to be the most interesting because it permits a good control over the size and morphology of the nanoparticles [9-10]. This is mainly due to the fact that the synthesis recipe is simple with one iron precursor, one type of organic ligand, and a high boiling point organic solvent. However at the same time, despite a lot of optimized synthesis reports, the influences of some synthesis parameters remain unclear such as the inert atmosphere in the three-neck flask during refluxing [11]. As observed with other synthesis routes, the magnetic moment of superparamagnetic iron oxide is much lower than that of bulk phase magnetite or its fully oxidized form: maghemite (γ-Fe$_2$O$_3$). Spin canted layer at the nanoparticle surface is reported as the main cause of it, but at the same time the presence of large number of defects and/or of a spin canting in volume is also not ignored. Therefore, along with the compositional control there is current requirement for the fine

[a] Department of Physics, H. P. University, Shimla 171005 HP India
[b] Centro Atomico Bariloche (CNEA), Instituto Balseiro (U. N. Cuyo) and Conicet, 8400 San Carlos de Bariloche, Río Negro, Argentina
[c] UGC DAE Consortium for Scientific Research, Indore 452001, India
[d] Núcleo de Pós-Graduação em Física, Campus Prof. José Aluísio de Campos, UFS, 49100-000 São Cristóvão, SE, Brazil
[e] Instituto de Física de La Plata (IFLP- CONICET), Universidade Nacional de La Plata (UNLP), c.c. 67, 1900 La Plata, Argentina
[f] Universidade Federal do Maranhão, Departamento de Física, 65080-805, São Luis, MA, Brazil, E. mail: surender76@gmail.com
†Electronic Supplementary Information (ESI) available: See DOI: 10.1039/x0xx00000x

structural and magnetic characterizations as a function of the nanoparticle size to establish size-dependent magnetic properties.

In the present paper, we have performed synthesis either in an inert atmosphere or in controlled vacuum in the three-necks round bottom flask on the phase purity of iron oxide nanoparticles (IONPs) and studied their magnetic properties. First synthesis has been performed out in an argon atmosphere, whereas the second one carried out in vacuum (10^{-2} mbar) through a simple rotary pump. The rest of the synthesis conditions were exactly same in both the cases. These nanoparticles have been investigated structurally and magnetically, through x-ray diffraction (XRD), high resolution transmission electron microscopy (HR-TEM), Soft X-ray absorption Spectroscopy (SXAS), Mössbauer spectroscopy (MS) at 300 K, and magnetic measurements in both ac and dc modes in order to correlate the structural and hence magnetic properties.

Experimental Section
Synthesis of iron oxide nanoparticles

The size of iron oxide nanoparticles (IONPs) has been controlled during synthesis by performing it in either inert atmosphere or vacuum using a standard inert gas/vacuum manifold system commonly known as Schlenk line. The synthesis were carried out in a standard three neck round bottom flask using thermal decomposition of Fe (acac) $_3$ (2.0 mmol) in the presence of 1-octadecene (20 ml) and the surfactants oleic acid (8 ml) and oleylamine (12 ml) either in pure Argon flux or vacuum. The above mixture was gently heated at 120^{0}C for 60 minutes under continuous argon or vacuum with intermediate stirring. The above mixture was slowly heated up to a final temperature of 315^{0}C for 60 minutes with heating rate of ~ 6 °C/min. The solution was then cooled down to room temperature under normal conditions and the nanoparticles were washed adding access of ethanol and centrifugation at 4500 rpm for 20 minutes. This procedure was repeated 3-4 times by dispersing the NPs in non-polar solvent, adding excess of ethanol and centrifugation. Finally, the nanoparticles were dispersed in toluene (concentration of 0.05 g/ml) for the long-term storage with 2-3 drops of oleylamine.

Characterizations

The particle diameter and its distribution were measured by means of HRTEM (200 keV JEM 2010 microscope) by drying a toluene dispersion of the nanoparticles on a carbon coated copper grid. The structure was determined by X-ray diffraction (XRD) (X´PERT Powder PANalytical) with Cu K$_\alpha$ radiations. The Rietveld refinement analysis of XRD patterns were performed using the DBWSTools2.3 refinement program [12, 13] A pseudo-Voigt function was selected to fit the observed peak profiles of the identified crystalline phase. The average crystallite size was calculated using all Bragg reflections by the Scherrer equation. The full width at half maximum (FWHM) of each peak was corrected with a standard sample of LaB$_6$. Further details of crystallite size calculation and profile function can be found in Ref. [14, 15]. Mössbauer spectrum was also measured
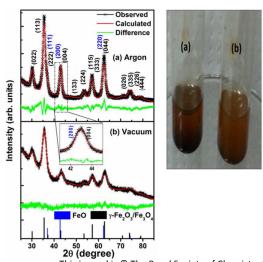
employing a homemade Mössbauer spectrometer working in a constant acceleration mode and equipped with a ^{57}Co (Rh) source with an activity of 50 mCi. The isomer shift values were referred to α-Fe foil at room temperature. X-ray absorption spectroscopy (XAS) measurements across Fe L$_{3,2}$ and O K-edge were performed at the SXAS beamline (BL-01) of INDUS 2 synchrotron source at RRCAT, Indore. XAS data were collected in total electron yield (TEY) mode at RT under ultra-high vacuum conditions. Pre and post edge correction of normalized XAS data were performed using Athena. The magnetic properties were measured on dried powder sample using SQUID (Quantum Design) magnetometer with fields up to 40 kOe and temperatures from 5-300 K. The ZFC and FC measurements were carried out as follow: the sample was first cooled down from 300 K to 5 K in a zero magnetic field, then a static magnetic field (*H* = 50 *Oe*) was applied and M_{ZFC} was measured during warming up from 5 *K* to 300 *K*; finally the sample was cooled down to 5 *K* under the same field and M_{FC} was measured during the cooling cycle. The real and imaginary parts of the ac magnetic susceptibility were measured at frequencies between 10 Hz < f < 10 kHz in external ac field amplitude of 10 Oe on a commercial Physical Property Measurement System (PPMS) in the temperature range 5-300 K.

Results and discussion

The phase purity and composition has been checked using powder XRD method and their Rietveld analysis. Figure 1 shows the powder XRD patterns for the two sample of iron oxide prepared under argon flux and vacuum. By analyzing the XRD patterns, it is confirmed that the brownish black powder obtained in case of sample prepared under argon consisted mainly of maghemite/magnetite (γ-Fe$_2$O$_3$/Fe$_3$O$_4$) (90(2) %) as well as wustite FeO phase (10(4) %), whereas the sample prepared under vacuum confirmed the formation of maghemite (γ-Fe$_2$O$_3$) as the major phase. Here we would like to mention that the most intense peaks of the FeO phase ({111}, $2\theta \cong 36.5^{o}$; {200}, $2\theta \cong 42.8^{o}$; {220}, $2\theta \cong 62.1^{o}$) are overlapped with the Bragg peaks {222}, {004} and {044} of the γ-Fe$_2$O$_3$/Fe$_3$O$_4$ phase. Thus, these peaks cannot be pulled apart among the others. However, the two major oxides of Fe namely maghemite (γ-Fe$_2$O$_3$) and magnetite (Fe$_3$O$_4$), are both cubic inverse spinels and structurally very similar to each other.

Figure 1 (left panel) X-ray diffraction patterns for iron oxide nanoparticles (IONPs) samples prepared under argon or vacuum conditions, (right panel)-showing the colloidal dispersion in toluene (a) argon, (b) vacuum condition. The labels indexed identify the miller indices (peaks most intense) of the phases γ-Fe$_2$O$_3$/Fe$_3$O$_4$ (in black) and FeO (in blue). The inset show the planes (200) and (004) of FeO and γ-Fe$_2$O$_3$/Fe$_3$O$_4$ phases, respectively.

Further from the XRD patterns, it is evident that the reflection lines are quite broad, suggesting the miniaturization of the powder crystallites into nanosized particles. Using the full width half the maximum (FWHM) and positions of the most intense peaks extracted from Rietveld refinement we have estimated the particle sizes. The average particle sizes were calculated without considering the possible contributions of crystal strain to the observed broadening by using Scherrer's equation;

$$D = \frac{k\lambda}{B\cos\theta} \tag{1}$$

where D is the average particle size, k is a shape factor for which a value of 0.9 is used and λ is the wavelength of the incident X-ray. Here B = $(B^2_M - B^2_S)^{1/2}$, where B_M is the FWHM of the XRD peak and B_S is the standard instrumental broadening. The average particle size calculated using eq. (1) are 7.4 nm and 5.1 nm for argon and vacuum condition, respectively and consists of nanosized particles for which superparamagnetic effects should be expected.

Figure 2 highlights the micro-structural features of both iron oxide nanoparticles. Here Figs. 2a, e display the representative low resolution TEM image for the IONPs synthesized in Argon atmosphere as well as in vacuum along with their high resolution images, respectively.
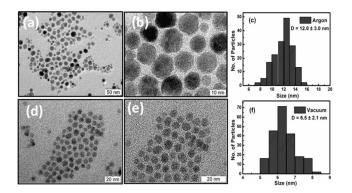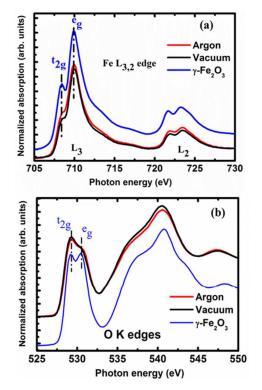

Figure 2 TEM images for iron oxide samples prepared in Argon atmosphere (a-c) and vacuum (d-f) along with their particle size distribution histograms.

In Fig. 2(b, e) the faceted-spherical shape can be clearly observed and we observed that there is no agglomeration among the particles owing to the organic capping on their surfaces. Evidently the nanoparticles obtained under argon atmosphere are more polydisperse as compared to the ones obtained under vacuum condition (Figure 2). The reason of this remarkable difference aforementioned synthesis paths are not clearly understood yet. The

detailed explanation of this issue is beyond the scope of this paper, where more systematic experiments at different vacuum levels are required as the boiling point of 1-octadecene changes as a function of atmospheric pressure. However, the vacuum path is promoting a narrower single-step process of nucleation and growth of nanoparticles, which means narrow particle size distribution. It is observed in the images (see Fig. 2a, b) that most of the particles show an inner contrast variation suggesting probably the existence of two phase structure consisting of γ-Fe$_2$O$_3$/Fe$_3$O$_4$ and FeO. Moreover, we have also seen the absence of such a contrast variation in most of the particles which could be explained by complete oxidation of those particles during the washing process or thereafter. Selected area electron diffraction (SAED) was also performed in order to see the crystallinity of the samples and the corresponding patterns are shown in ESI Figure S1. However, it was not possible to quantify the interplanar distance of each electron diffraction ring, but the observed results hints towards a better crystallinity of both the samples.

It is not very straightforward to distinguish between two forms iron oxide namely maghemite (γ-Fe$_2$O$_3$) and magnetite (Fe$_3$O$_4$) from the XRD patterns, therefore x-ray absorption spectroscopy has been used to understand the oxidation states of Fe for these two samples. Figure 3 shows X-ray absorption near edge spectra (XANES) across Fe L$_{3,2}$ edges (fig 3(a)) and O K edges (fig 3(a)) for iron oxide nanoparticles along with reference compound γ-Fe$_2$O$_3$.

Figure 3 (a) Fe L$_{3,2}$ edges and (b) O K edges XANES recorded in TEY mode for iron oxide nanoparticles prepared in argon atmosphere, and vacuum conditions along with reference compound γ-Fe$_2$O$_3$.

Fe $L_{3,2}$ edge XANES probes the unoccupied 3d states of Fe via electron transitions from spin orbit split levels $2p_{3/2}$ to 3d (L_3 edge) and $2p_{1/2}$ to 3d (L_2 edge). Due to crystal field splitting L_3 and L_2 edges are further split into t_{2g} and e_g levels (marked for L_3 edge). A careful observation of L_3 edge shows that t_{2g} feature is suppressed in nanoparticles; suppressed relatively more in the nanoparticles prepared in vacuum. Weaker (stronger) t_{2g} feature in L_3 edge of Fe is indicative of less (more) un-occupancy in t_{2g} state, which is the case for Fe^{2+} (Fe^{3+}), so supporting the situations for Fe_3O_4: Fe^{2+}& Fe^{3+} (γ-Fe_2O_3: only Fe^{3+}). Slightly increased t_{2g} feature for nanoparticles prepared in argon is indicative of increased Fe^{3+} content (indicative of presence of γ-Fe_2O_3). Oxygen K edge features here are clearer for disentangling the γ-Fe_2O_3 and Fe_3O_4 phases. Features at around 530 eV in XANES at O K edge probes the transition of O 1S electrons in to O 2p states (hybridized with Fe 3d states, split into Fe t_{2g} and e_g states) [16]. While features above 535 are O 1s electrons' transitions into O 2p states hybridized with Fe (4s,4p) states [16].Intensity ratios of t_{2g} and e_g features (~ 530 eV) for vacuum nanoparticles mimics the O K edge feature of Fe_3O_4, reported in literature [17]. Features t_{2g} and eg in argon nanoparticles show deviation from Fe_3O_4 feature and tendency of γ-Fe_2O_3 features, due to presence of slight admixture of γ-Fe_2O_3.

[57]Fe Mössbauer spectroscopy is a powerful tool to characterize IONPs undergoing superparamagnetic (SPM) relaxation. Figure 4 shows the Mössbauer spectra recorded for the two samples at 300 K, while the values of the Mössbauer hyperfine parameters, derived from the fitting of the recorded Mössbauer spectra, are listed in Table 1. Here, the dots in Fig. 4 represent the experimental data and solid lines through data points are least squares fittings. The 300 K Mössbauer spectrum of the both samples shows relaxation effects owing the nanometric particle size. In both samples a doublet contribution corresponding to superparamagnetic is recognize. The sample prepared in argon atmosphere, according with its bigger size, also presents a distributed sextet component characteristic of collective magnetic excitation (CME) phenomena. In this case, the fitting was made using one distribution of hyperfine fields and one doublet. The corresponding values of the Mössbauer hyperfine parameters (see Table 1), in particular the isomer shift values, are typical of high-spin Fe (III) atom in iron (III) oxides [18]. There is no indication of presence of the Fe^{2+} valence state, which confirms that both samples are solely of Fe_2O_3 origin.

Table 1 Values of the Mössbauer hyperfine parameters, derived from the Mössbauer spectrum recorded 300 K, where isomer shift (IS), quadrupole splitting (QS), mean magnetic hyperfine field (B_{hf}), relative area % and assignments of individual spectral components are shown.

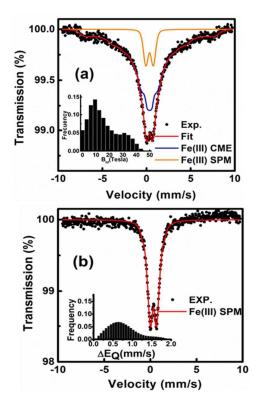| Sample	Component (Area)	IS (±0.01 mm/s)	QS (±0.01 mm/s)	B_{hf} (±0.1T)	Assignment
Argon	Doublet (14%)	0.34	0.84	-	Fe^{3+} SPM component
	Sextet (86%)	0.34	-	15.8	Fe^{3+} CME component
Vacuum	Doublet (100%)	0.33	0.85	_	Fe^{3+} SPM component

Figure 4 Mössbauer spectra for the iron oxide nanoparticles at 300 K prepared in (a) argon atmosphere, and (b) Vacuum conditions.

This is quite expected in connection with their nano size with a large surface-to- volume ratio securing their complete oxidation during the synthesis. On the timescale of the Mössbauer spectroscopy, the nanoparticles of both samples presents thermally induced reversal of its magnetization direction at 300 K. Here, the doublet component belongs to the nanoparticles with thermally fluctuating super spins having relaxation times much smaller than the characteristic measurement time (τ_m) of the Mössbauer spectroscopy, i.e. superparamagnetic relaxation; while the presence of a distributed sextet component corresponds to nanoparticles whose super spin thermally fluctuates between the energetically favored orientations with a relaxation time close to τ_m, i.e. collective magnetic excitations. These two samples would show superparamagnetic features in their dc magnetization measurements at 300 K, however, this will be largely driven by finite-size and surface effects which can depicted by a smaller saturation moment or lack of full saturation etc.

Further, we have performed magnetization (M) measurements as function of both temperature (T) and as well as applied magnetic field (H). Figure 5 shows the variation of M as a function of T in the range 5 - 300 K in an external magnetic field of 50 Oe recorded in zero-field-cooled (ZFC) and field-cooled (FC) modes for both the samples.
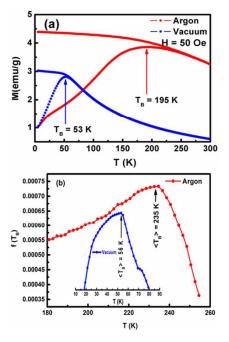
Figure 5 (a) Zero-field-cooled (ZFC) and Field-cooled (FC) curves for the iron oxide sample, (b) the mean blocking temperature calculated from the distribution of blocking temperatures

In the ZFC curves, a characteristic superparamagnetic (SPM) peak confirms the nanoscale nature of iron oxide particles. In addition, the separation of ZFC and FC curves at a certain irreversibility T_{IRR} temperature is one of the characteristic features of SPM. The maximum observed in the ZFC curves T_{MEAN} (related to the mean blocking temperature T_B) is slightly lower than T_{IRR}. Such behavior indicates a particle size distribution, whereas a fraction of the largest particles already freezes at T_{IRR}, the majority fraction of the nanoparticles is being blocked at around T_{MEAN}. It is evident from Fig.5(a) that there is a sharp maximum in M_{ZFC} curve (~ 53 K for the sample prepared under vacuum as compared to other prepared in Argon atmosphere which is ~ 195 K), which indicates their mean blocking temperatures. Furthermore, the relatively sharpness of the ZFC curve peak for the sample prepared under vacuum and the fact that T_{IRR} and T_{MEAN} are quite close to each other (T_{IRR} ~60 K) can be taken as an indication of a narrow size distribution for this sample. It is worth mentioning that the generally distribution of blocking temperatures($f(T_B)$) can be calculated as the temperature derivative of the difference between the M_{FC} and M_{ZFC} magnetizations ($d[M_{FC}-M_{ZFC}]$)/dT, allowing one to estimate correctly the mean blocking temperature $<T_B>$ [19-20]. The $<T_B>$ calculated from the distribution of blocking temperatures was found to be ~ 56 K and ~ 235 K (see Fig. 5b) for the sample prepared in vacuum and argon atmosphere, respectively. From the $<T_B>$, we have calculated the mean size using the Néel relaxation model for isolated particles, *i.e.*, $D=[(6k_B<T_B>\ln(t_mf_0)/\pi K_{eff}]^{1/3}$, where K_{eff} is the anisotropic energy of iron oxide, t_m the measurement time, f_0 is the frequency factor and D is the size of iron oxide nanoparticles. Considering the value 2×10^4erg/cm^3, 100 s, and 10^9 s^{-1} for K_{eff} for cubic iron oxide (Fe$_3$O$_4$

or γ-Fe$_2$O$_3$), t_m, and f_0, respectively, a value of 9.2 nm (argon) and 5.6 nm (vacuum) are obtained for the iron oxide nanoparticles, which are in a good agreement with XRD and TEM findings.
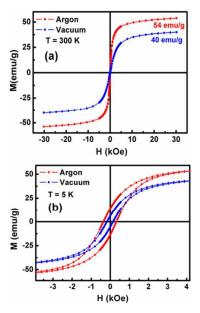

Figure 6 MH curves for the iron oxide samples at (a) 300 K, (b) 5 K

The magnetization hystersis loops recorded at 300 K and 5 K in ZFC mode. At 300 K, the sample shows zero coecivity and retentivity, indicating that the particles are in SPM state without saturation up to a field of 30 kOe, whereas at 5 K, the coercivity is ~ 345 Oe and ~165 Oe for the sample prepared in argon and vacuum condition, respectively. This can also be explained due to the fact that γ-Fe$_2$O$_3$ is magnetically softer than Fe$_3$O$_4$. Additionally, coexisting phases could induce more magnetic frustration than single magnetic phase, thereby inducing an increment of the coercivity for the sample prepared in argon atmosphere against the vacuum one. The saturation magnetization (M_S) of the sample prepared under vacuum is smaller than the one prepared under argon and bulk γ-Fe$_2$O$_3$. Roughly, this can be explained due to the fact the M_S value of bulk γ-Fe$_2$O$_3$ (76 emu/g@293 K) is smaller than the value of Fe$_3$O$_4$, (93 emu/g@290 K) [21]. Here we note that nanoparticles prepared under vacuum are majority composed of γ-Fe$_2$O$_3$, whereas nanoparticles prepared under argon are of multi-phase composition with majority of γ-Fe$_2$O$_3$/Fe$_3$O$_4$. Reduced M_S compared to bulk values are commonly ascribed to spin canting or defects at the particle's outer surface [21]. Indeed, previous work has identified iron oxide nanoparticles that can be composed of Fe$_{3-\delta}$O$_4$, for example, which is a solid solution of the end members Fe$_3$O$_4$ and γ-Fe$_2$O$_3$ (both ferrimagnets, FiM); Fe$_{1-x}$O (wüstite) an antiferromagnet, AFM; or Fe, a ferromagnet, FM. Further, we have measured the hysteresis curves for both the samples at 5 K in a field cooled (H_{FC} = 70 kOe) mode for both the samples (figures not shown here) and observed that the sample prepared in argon atmosphere displayed a measurable exchange bias of ~ 40 Oe at 5 K, whereas the hysteresis curve for the sample prepared under

vacuum is symmetric about the origin. This further confirms the presence of exchange coupling between maghemite (ferromagnetic) and wustite (antiferromagnetic) phase for the sample prepared in argon atmosphere.

To have a deeper insight about these two samples, we have further performed temperature dependence of dc magnetization after ZFC and FC at different magnetic fields. It is observed that the magnetization increases with increasing magnetic field, while the T_B shifts to lower temperatures with increasing magnetic field, indicating the frozen spin glass state is gradually destroyed under large magnetic fields for both samples (see Figure 7 and 8). This coincides well with the bother SG systems [22-25].
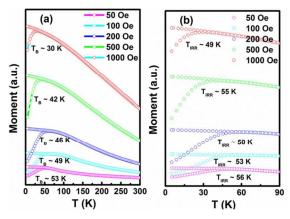

Figure 7 (a) T- dependent magnetization $M (T)$ curves under FC and ZFC modes with different magnetic fields magnetization curves measured under different magnetic fields up to 1 kOe, and (b) its enlarged view for the sample prepared under Argon flux.
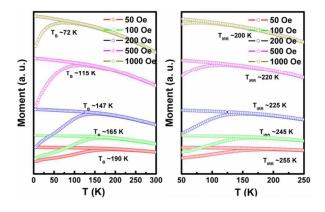

Figure 8 (a) T- dependent magnetization $M (T)$ curves under FC and ZFC modes with different magnetic fields magnetization curves measured under different magnetic fields up to 1 kOe, and (b) its enlarged view for the sample prepared under vacuum condition.

We have further investigated the temperature dependence of the ac susceptibility measurements at different driving frequencies in the range from 10 Hz-10 kHz (see Fig. 9(a-b)) for both samples prepared under argon flux or vacuum conditions. It is observed that χ' (T) exhibits a strongly frequency dependent peak. As the

frequency increases, the sharp peak shifts to higher temperatures, while the height decreases, suggesting a characteristics feature of typical SG behavior. The expected behaviour of blocking processes is evident in the plots, *i.e.* the occurrence of a maximum at T_B, which shifted towards higher temperatures and decreased in height with increasing frequency [26]. The effect that becomes visible upon sample cooling is directly related to the frequency dependence of T_B of the single-domain particles. Two key empirical relations are often used as tools to compare the frequency dependence of T_B namely, $C_1 = \Delta T_B/T_B\Delta log_{10}(f)$, independent of any model and $C_2 = (T_B-T_0)/T_B$, where ΔT_B is the difference between the T_B measured in the $\Delta log_{10} (f)$ frequency interval and f represents the ac magnetic field frequency [26]. The parameters C_1, C_2 and T_0 deliver a model-independent classification of the blocking/freezing process [26-28].
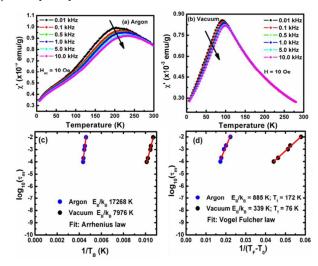

Figure 9 (a-b) T-dependence of the real part of the ac susceptibility for the prepared under argon and vacuum, respectively, at different frequencies. Arrow indicates increasing frequencies. (c) & (d) variation of T_B in the classical Arrhenius and Vogel-Fulcher plot of $log_{10} (\tau)$ vs. 1/T

This law is phenomenological and without physical significance near T_0, and yet C_2 can be taken as indicator to screen different T_B in closely related materials. Figure 9(c) shows the variation of the T_B in the classical plot of $log_{10}(\tau)$ vs. 1/T_B for both samples. For isolated nanoparticles, f-dependence of the T_B has been predicted, according to the SPM Neel model, to follow an Arrhenius law $ln(\tau/\tau_0) = E_B/kT_B$, where $\tau =1/f$, τ_0 is the characteristic relaxation time constant (10^{-9} s $<\tau_0<10^{-12}$ s), and E_B is the energy barrier of the NPs for the moment reversal [27]. Thus, $E_B= KV$, and K represents the effective anisotropy constant and V the volume of the particle. The terms E_B and K can be estimated from analyses of the experimental data. Even though the fitted straight-lines in Fig. (9c) seem to well support the experimental findings; the fitted parameters obtained had no physical meaning for both the samples. Particularly, the τ_0 values in both samples were found much smaller than those physically accepted, and E_B values were found too high as compared to the reference values of E_B= 8440 K

for iron oxide (calculated using $K = 5.5 \times 10^6$ erg/cm^3). Thus, the experimentally observed variations in $\chi'(T)$ for these samples were not consistent with the simple superparamagnetic blocking behaviour of independent particles. The data were then analysed by using the Vogel-Fulcher relation [26] and can be written as $\tau = \tau_0 exp\{E_A/k_B(T_B - T_0)\}$. Here T_0 is an effective temperature with similar origin to that used to reproduce the dc susceptibility in the superparamagnetic regime and T_B is the characteristics temperature signaling the onset of the blocking process.

Taking into account Vogel-Fulcher relation, the calculated fitted parameters are given in Fig. 9d, and can be compared with the values extracted by using the Néel-Arrhenius relation. The Vogel-Fulcher law provides more reasonable values of τ_0 and E_B for both samples, comparable to those observed for spin-glass (SG) systems [26]. For sample prepared under Argon flux, the energy barrier (E_B/k_B) and effective temperature is enhanced by more than two times in comparison to vacuum one , ($T_0 = 76$ K for vacuum, $T_0 = 172$ K for Argon). In this case, the VG fitting is giving the following values of the parameters: $\tau_0 = 1.0 \times 10^{-10}$ s, $T_0 = 76$ K and $\tau_0 = 5.0 \times 10^{-12}$ s, and $T_0 = 172$ K, respectively for the sample prepared in vacuum and argon atmosphere, respectively. A good agreement of the experimental data and Vogel-Fulcher (VG) law evidences that the phenomenon taking place at maximum of susceptibility is related to blocking of an assembly of interacting particles rather that a collective freezing as that occuring in a spin-glass system.

Conclusions

Synthesis method clearly shows the effect of argon and vacuum environments on the structure-property relationship of iron oxide nanoparticles. Detailed XRD, XANES and Mössbauer experiments suggest that the dominating chemical phase is γ-Fe$_2$O$_3$ for both the samples. Vacuum conditions result in narrow particle size distribution as compared to argon atmosphere. DC magnetization measurements revealed that nanoparticles are superparamagnetic above the blocking temperature. However, the analysis of ac susceptibility data shows that magnetic dynamics of these nanoparticles is strongly influenced by spin-glass features and is well described by the Vogel-Fulcher (VG) law for interacting superparamagnetic particles. On the other hand, endeavor to fit the data with Neel-Brown (NA) model for thermally non-interacting superparamagnetic (SPM) particles is unsuccessful and yields an unphysical small value of relaxation time constant τ_0.

Acknowledgements

References

1 B. Z. Zeng, and S Sun, Adv. Funct. Mater. 2008 **18** 391.
2 Y. Hou, Z. Xu, and S. Sun, Angew. Chem. Int. Ed. 2007 **46** 6329.
3 C. J. Chen, R. K. Chiang, H. Y. Lai, and C. R. Lin, J. Phy. Chem. C 2010 **114** 4258.
4 Yu. S. Dedkov, U. Rudiger, and G. Guntherodt, Phys. Rev B. 2002 **65** 064417.
5 P. Seneor, A. Fert, J. L. Maurice, F. Montaigne, F. Petroff, and A. Vaures, Appl. Phys. Lett. 1999 **74** 4017.
6 A.K. Gupta, and S. Wells, IEEE Trans Nanobiosci 2004 **3** 66.
7 S. W. Charles, Magnetic fluids (ferrofluids). *In: Dormann JL, Fiorani D*, editors. Magnetic properties of fine particles. North Holland: Elsevier; 1992. p. 267–374.
8 A. K. Gupta, and A. S. G. Curtis, Biomaterials, 2004 **25** 3029.
9 S. K. Sharma**,** J. M. Vargas, N. M. Vargas, S. C. Sepúlveda, D. Altbir, K. R. Pirota, R. Zboril, G. Zoppellaro and M. Knobel, RSC Advances, 2015 **5** 17117.
10 S. K. Sharma, J. M. Vargas, Shalendra Kumar, C. G. Lee, K. R. Pirota, and M. Knobel, J. Alloys & Compd., 2011 **509** 6414.
11 W. Wu, Z. Wu, T. Yu, C. Jiang, and W.S. Kim, Sci. Technol. Adv. Mater. 2015 **16** 023501
12 R.A. Young, A. Sakthivel, T.S. Moss, C.O.P. Santos, J. Appl. Crystallogr. 1995 **28** 366
13 L. Bleicher, J. M. Sasaki, and C. O. P. Santos, J. Appl. Cryst. 2000 **33** 1189.
14 C. T. Meneses, W. H. Flores, F. Garcia, and J. M. Sasaki, J. Nanoparticle Research 2006 **9** 501.
15 R. A. Young, The Rietveld Method, Oxford Science Publications, p. 126, New York, 1993.
16 F. M. F. de Groot, M. Grioni, J. C. Fuggle, J. Ghijsen, G. A. Sawatzky, and H. Petersen, Phys. Rev. B, 1989 **40** 5715.
17 Wei-Cheng Wang, Shih-Yun Chen, Per-Anders Glans, Jinghua Guo, Ren-Jie Chen, Kang-Wei Fong, Chi-Liang Chen, Alexandre Gloter, Ching-Lin Chang, Ting-Shan Chan, Jin-Ming Chen, Jyh-Fu Lee, and Chung-Li Dong, Phys. Chem. Chem. Phys., 2013 **15** 14701.
18 R. M. Cornell, and U. Schwertmann, The Iron Oxides: Structure, Properties, Reactions, Occurrence and Uses, Wiley VCH, Weinheim, Germany, 2003;
J. A. Ramos Guivar, A. Bustamante, J. Flores, M. Mejía Santillan, A. M. Osorio, A. I. Martínez, L. De Los Santos Valladares, and C. H. W. Barnes, Hyperfine Interactions 2014 **224** 89.
19 S. Barzilai, Y. Goldstein, I. Balberg, and J. S. Helman, Phys. Rev. B 1981 **23** 1809.
20 J. C. Denardin, A. L. Brandl, M. Knobel, P. Panissod, A. B. Pakhomov, H. Liu, and X. X. Zhang, Phys. Rev B 2002 **65** 064422.
21 E. Wetterskog, C. W. Tai, J. Grins, L. Bergstrom, and G. S. Alvarez, ACS Nano, 2013 **7(8)** 7132.
22 B. Song, J. K. Jian, H. Q. Bao, M. Lei, H. Li, G. Wang, Y. P. Xu and X. L. Chen, Appl. Phys. Lett., 2008 **92** 192511.
23 B. S. Wang, P. Tong, Y. P. Sun, X. B. Zhu, Z. R. Yang, W. H. Song and J. M. Dai, Appl. Phys. Lett., 2010 **97** 042508.
24 X. H. Zhang, Q. Yuan, J. C. Han, J. G. Zhao, J. K. Jian, Z. H. Zhang and B. Song, Appl. Phys. Lett., 2013 **103** 022405.
25 S. K. Sharma, R. Kumar, S. Kumar, M. Knobel , V. V. Siva Kumar, V. R. Reddy, M. Singh, and C. G. Lee, J. Phys. Cond. Mater. 2008 **20** 235214.
26 J. M. Vargas, A. Srivastava, A. Yourdkhani, L. Zaldivar, G. Caruntu, and L. Spinu, J. Appl. Phys. 2011 **110** 064304.

27 M. Knobel, W. C. Nunes, L. M. Socolovsky, E. De. Biasi, J. M. Vargas, and J. C. Denardin, J. Nanosci. Nanotechnol. 2008 **8** 2836.

28 J. L. Dormann, L. Bessais, and D. Fiorani, J. Phys. C: Solid State Phys. 1988 **21** 2015.